Preparation of methylammonium lead iodide (CH₃NH₃PbI₃) thin film perovskite solar cells by chemical vapor deposition using methylamine gas (CH₃NH₂) and hydrogen iodide gas

Claudiu Mortan[1] | Tim Hellmann[1] | Moritz Buchhorn[1] | Marco d'Eril Melzi[1] | Oliver Clemens[2] | Thomas Mayer[1] | Wolfram Jaegermann[1]

[1]Department of Surface Science, Institute for Material Science, Technical University of Darmstadt, Darmstadt, Germany

[2]Department of Material Design Through Synthesis, Institute for Material Science, Technical University of Darmstadt, Darmstadt, Germany

Correspondence
Claudiu Mortan, Department of Surface Science, Institute for Material Science, Technical University of Darmstadt, Otto-Berndt-Str. 3, 64287 Darmstadt, Germany.
Email: cmortan@surface.tu-darmstadt.de

Abstract

An upscalable chemical vapor deposition setup has been built-up and employed in producing methylammonium lead iodide (MAPI) thin film perovskite solar cells, leading to a maximum efficiency of 12.9%. The method makes use of methylamine gas and hydrogen iodide gas to transform a predeposited layer of lead(II)iodide (PbI_2) into MAPI. Although the reaction mechanism includes the intermediate phases lead oxide (PbO) and lead hydroxide ($Pb(OH)_2$), indicated at least on the surface of the samples by XPS, neither species could be observed in XRD measurements of the stepwise reaction, which show a mixture of highly oriented cubic and tetragonal MAPI perovskite lattice systems.

KEYWORDS
chemical vapor deposition, chemistry, emerging photovoltaics, engineering, materials science, methylammonium lead iodide, perovskite, solar cells, sustainable energy, thin films

1 | INTRODUCTION

Since their emergence in 2012,[1,2] thin film organometal halide perovskite solar cells have experienced a uniquely fast improvement in certified efficiency of up to 25.2% in 2020.[3] Complementing silicon (Si) solar cells in tandem device structures, a certified efficiency of 29.1% has been achieved to date,[4] paving the way to reaching the current optimized efficiency of the best double-junction tandem solar cells of 32.9%,[5] that already overcomes the Shockley-Queisser limit of single-junction solar cells.[6] Challenges like reducing the environmental impact, increasing the stability, and reducing the cost of production even further remain. Popular routes to
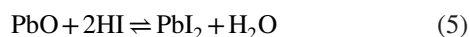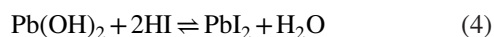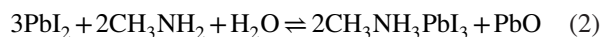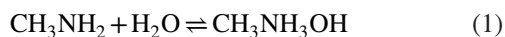
forming the photo-active perovskite methylammonium lead iodide (CH₃NH₃PbI₃, MAPI) is either from solution, by spin coating, or from the gas phase, by evaporating the two precursor salts lead(II)iodide (PbI_2) and methylammonium iodide, (CH₃NH₃I, MAI). Since CH₃NH₃I can decompose to either ammonia (NH_3) and methyl iodide (CH₃I),[7] or to methylamine (CH₃NH₂, MA) and hydrogen iodide (HI),[8] a chemical vapor deposition (CVD) route to forming MAPI perovskite would seem possible, by mixing either combinations of the decomposition precursors with lead(II)iodide. The standard route to synthesize the MAI salt is by mixing an ethanol, or methanol MA solution with hydroiodic acid, HI (aq.).[9-11] For further purification and recrystallization, a considerable

amount of solvents like diethyl ether or isopropanol are used. Synthesizing MAPI from PbI_2 by directly using the two gases MA and HI with the respective boiling temperatures of $-6°C$ and $-35°C$ would thus be an alternative route. An industrially established process that could achieve this would thus be within reach, through the development of a highly upscalable CVD process.

Zhou et al[12] was one of the first to report the use of MA for healing MAPI perovskite films, describing the formation of a $CH_3NH_3PbI_3 \cdot xCH_3NH_2$ liquid phase during the perovskite-gas interaction. Raga et al[13] reported shortly after a synthetic route to forming MAPI perovskite thin films that implies exposure of a PbI_2 film to an atmosphere of heated methylamine from ethanol on a hot plate, in combination with an atmosphere of heated hydroiodic acid (HI aq.). They achieved an efficiency of 12.7% with a sequential process and 15.3% with a simultaneous HI + MA process. The paper established a reaction mechanism between the MA, HI, and PbI_2, as shown by the Equations 1-5. Water from the atmosphere is needed for the reactions in Equations 1 and 2 to take place. In the MA step, Equations 2 and 3, the formation of lead oxide (PbO) and lead hydroxide $Pb(OH)_2$ can be observed. These species would be regenerated to lead iodide (PbI_2) in the HI step, according to Equations 4 and 5.

$$CH_3NH_2 + H_2O \rightleftharpoons CH_3NH_3OH \quad (1)$$

$$3PbI_2 + 2CH_3NH_2 + H_2O \rightleftharpoons 2CH_3NH_3PbI_3 + PbO \quad (2)$$

$$3PbI_2 + 2CH_3NH_3OH \rightleftharpoons 2CH_3NH_3PbI_3 + Pb(OH)_2 \quad (3)$$

$$Pb(OH)_2 + 2HI \rightleftharpoons PbI_2 + H_2O \quad (4)$$

$$PbO + 2HI \rightleftharpoons PbI_2 + H_2O \quad (5)$$

2 | MATERIALS AND METHODS OF CHARACTERIZATION

2.1 | Glass coated with fluorine-doped tin oxide (FTO)

Pilkington NSG TEC15 FTO glass substrates have been used, cut as 2 cm × 2 cm squares, with a sheet resistance of 12-14 Ω/sq. and a thickness of 2.2 mm.

2.2 | c-TiO₂ layer

The compact TiO_2 layer is produced by spray pyrolysis on the glass/FTO substrates. Five hundred microlitre of titanium diisopropoxide bis(acetylacetonate), 75 wt. % in isopropanol (TIAA) from Merck, is mixed with 18 mL reaction grade Ethanol. This solution is sprayed using oxygen carrier gas onto the glass/FTO substrates that have been treated for 5 minutes in an oxygen plasma oven and heated to 450°C for 25 minutes prior to deposition. After the spraying process, the substrates are sintered for 30 minutes at 450°C in atmosphere.

2.3 | m-TiO₂ layer

The mesoporous TiO_2 layer is deposited by spin coating 100 μL of a 1:7 weight ratio solution of 18NR-T Titania (TiO_2) paste from Greatcell Solar and reaction grade ethanol onto each glass/FTO/c-TiO_2 substrates in atmospheric conditions. The solution is dropped on a substrate, before spinning at 83 rps (revolutions per second) for 45 seconds. After drying for 10 minutes at 70°C, an additional sintering step takes place for 45 minutes at 450°C on a hot plate, in atmospheric conditions.

2.4 | PbI₂ layer

Prior to the deposition of the lead(II)iodide layer, the glass/FTO/c-TiO_2/m-TiO_2 substrates are treated in a UV/ozone oven for 15 minutes. The deposition takes place in a nitrogen (N_2)-filled glovebox. After each substrate has been heated for 2 minutes at 80°C on a hot plate, 100 μL of a 555 mg PbI_2 (Alfa Aesar 99.9985%, metal base) in 1 mL DMF (*N,N*-Dimethylformamide, Merck, 99.8%, anhydrous) solution that has been stirred for at least half an hour at 80°C is dropped onto the hot substrates, then spun at 108 rps for 90 seconds. Each substrate is dried for 10 minutes at 80°C.

2.5 | Methylamine gas

CH_3NH_2 in steel lecture bottle, Merck, 99.0%.

2.6 | HI gas

Hydroiodic acid, Merck, 57 wt., % in H_2O, distilled, stabilized 99.95%. Iodine, Laborladen, double sublimated. Red phosphorous, Laborladen, min. 98%.

2.7 | Spiro-MeOTAD layer

The deposition of the spiro-MeOTAD layer takes place in a nitrogen (N_2) glovebox. Eighty milligram spiro-MeOTAD

(Borun New Material, 99.9%) is mixed in 1 mL chlorobenzene (Merck, anhydrous, 99.8%) with 28.5 μL 4-tert-butylpyridine (Merck, 98%) and with 17.5 μL of a solution made from 260 mg Li-TFSI (bis(trifluoromethane)sulfonimide lithium salt, Merck, >99%) and 0.5 mL acetonitrile (Merck, anhydrous 99.8%). One hundred microlitre of the resulted spiro-MeOTAD solution is dropped on a glass/FTO/c-TiO$_2$/m-TiO$_2$/MAPI substrate. After a pause of 20 seconds, it is spun at 23 rps for 30 seconds and left to dry at room temperature in the glovebox.

2.8 | Gold layer

The front contact of the substrate is cleaned of the excess material through rubbing off with a cotton swab, dipped in isopropanol until transparent. The gold (Au) layer is deposited by argon sputtering in a Quorum Technologies Q300TD machine with 30 mA current for 120 seconds, using a steel mask.

2.9 | XRD setup

X-ray diffraction (XRD) patterns were recorded on a Bruker D8 Advance in Bragg-Brentano geometry with Cu Kα radiation and a VANTEC detector. The samples were measured in a 2θ-range between 10° and 90° using a fixed divergence slit of 0.3° for 60 minutes All samples were measured at ambient atmosphere, at most within few hours after production.

2.10 | XRD refinements

Analysis of diffraction data was performed using the Rietveld method with the program TOPAS V. 5.0 using the whole 2θ-range (10°-90°). The instrumental intensity distribution of the instrument was determined empirically from a sort of fundamental parameters set 27, using a reference scan of LaB$_6$ (NIST 660a) and silicon, respectively. The texture parameters required to fit the perovskite phases were calculated by application of the March model,[14] in relation to the (100) plane for the cubic phase, or the (100)(001) planes for the tetragonal model.

2.11 | XPS setup

We used a ThermoFisher Scientific ESCALAB 250X. Mg K$_α$ radiation with an excitation energy of 1254 eV and a take-off angle of 90°. The machine was calibrated using copper, gold, and silver standards.

2.12 | SEM setup

An FEI/Philips scanning electron microscope was used, of model FEX XL 30, that has a Schottky-type electron source and is equipped with an Everhart-Thornley secondary electron (SE) detector. The samples are tilted at 70°.

2.13 | UV-/Vis setup

Perkin Elmer Lambda 900, using an Ulbricht sphere and calibrated using barium(II)sulfate (BaSO$_4$) in a total reflection approach.

2.14 | PL setup

Varian Cary Eclipse, 350 nm excitation with Schott WG 11, 3 mm filter and Schott GG 450 nm as an emission filter.

2.15 | Solar simulator setup

The solar simulator is built by LOT Quantum Design, LSH102, using a USHIO UXL-150SO-Xenon Lamp and an AM 1.5G (air mass, global) filter. The samples were measured unmasked. The area of the cells was defined by the gold back contact.

3 | CHEMICAL VAPOR DEPOSITION SETUP

The CVD setup used in this work allows the transformation of a lead iodide (PbI$_2$) thin film to MAPI (methylammonium lead iodide, CH$_3$NH$_3$PbI$_3$), in a multi-step cycled process, that involves the precursor gases methylamine (CH$_3$NH$_2$, short MA) and hydrogen iodide (HI). A photograph of the setup, built-up in a laboratory hood, can be seen in Figure 1. Figure 2 features a schematic drawing of its components. The main body consists of a three-zone tube furnace equipped with infrared heaters and a reaction glass tube with KF (klein flange) vacuum flanges. The temperature in each zone can be controlled by feedback loops of K-type thermocouples with feedthroughs inside the glass tube. Metal holders as seen in Figure 3 can hold up to three substrates, stacked vertically. In this setup, different types of gases can be inserted into the reaction tube, the pressure of which can be monitored using a Bourdon pressure gauge. Surrounding air or nitrogen is filled in by a manually controlled ball valve. Methylamine gas can be dosed using a standard steel lecture bottle with a

manual pressure regulator. The HI gas is self-made using a glass apparatus connected to the reaction tube, by adding hydroiodic acid, mixed with a surplus of iodine, from a dropping funnel to red phosphorous.[15] The evolving HI gas is optionally passed through the drying agent phosphorus pentoxide (P_4O_{10}) before entering the reaction tube, removing further water vapor from the formed gas, to promote the formation of the right side of Equations 4 and 5, according to Le Chatelier's equilibrium law. The complete setup can be evacuated to ca. 1 mbar with the help of a rotary vane pump. A manual membrane valve is used to disconnect the vacuum line from the reaction tube. To hinder condensation of the reactive gases inside the rotary vane pump, a cold trap with liquid nitrogen (LN_2) is connected between the reaction tube and the pump.

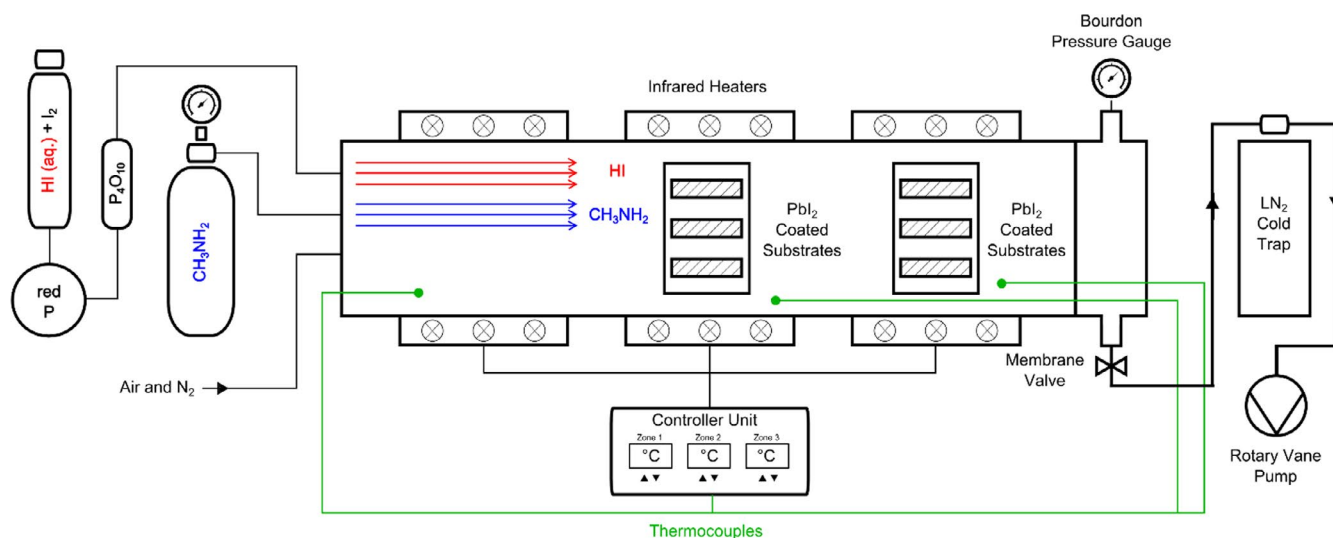**FIGURE 1** Chemical vapor deposition setup

4 | CVD PROCEDURE

For transforming PbI_2 to MAPI, MA and HI are introduced in the reaction tube sequentially and in multiple cycles. A half cycle (0.5, 1.5, and 2.5) refers to a methylamine step, and a whole cycle (1.0 and 2.0) refers to an HI step. Prior to loading the spin-coated PbI_2 samples, the reaction tube is heated to 100°C for at least an hour under vacuum to remove any residuals that may adhere to the walls. All further steps take place at room temperature. For the methylamine step, 400 mbar of surrounding (humid) air is introduced into the reaction tube. After inserting an additional 200 mbar of methylamine, the yellow PbI_2-coated substrates turn transparent, as seen in Figure 3.

Very small droplets can be observed on the surface that indicate a formed liquid phase of the methylamine and PbI_2 complex.[16-18] This intermediate phase is one of the advantages of the methylamine process, since the resulting film becomes very smooth, independent of the roughness of the initial precursor layer of PbI_2, as shown by the SEM images in Figure S2. After 15 seconds, a 600 mbar air flow for 1 minutes removes the methylamine gas from the tube. In the first seconds of removing the methylamine gas, the substrates turn light brown, with gradual darkening. To remove all excess methylamine and air from the reaction tube, it is purged three times with nitrogen (1 bar to 1 mbar). In the next step, 200-300 mbar of HI gas is added to the evacuated tube. To produce the HI gas, 57 wt. % concentrated hydroiodic acid is mixed with solid iodine in a 1:2 weight ratio. The solution is dropped onto red phosphorous[15] and the resulting HI gas is optionally passed through the drying agent phosphorous pentoxide (P_4O_{10}), to further remove excess water vapor. After 10 minutes reaction time, the HI gas is removed by purging three times with nitrogen. After evacuating, the methylamine and HI steps are repeated for 2.5 cycles.
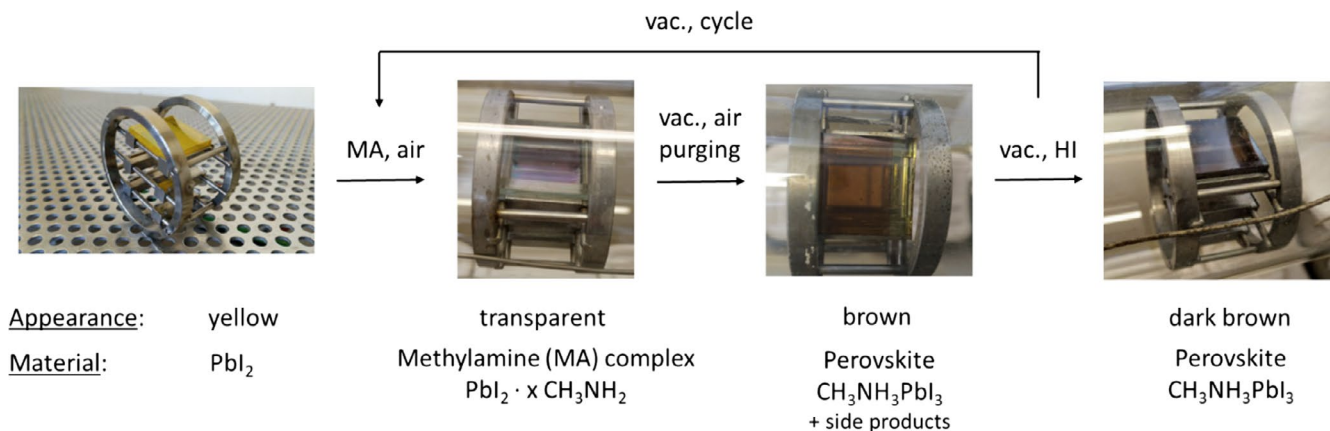

FIGURE 2 Schematic draft of the chemical vapor deposition setup

FIGURE 3 Process diagram of the chemical vapor deposition process with images of the intermediate stages

5 | RESULTS AND DISCUSSION

The substrates of the intermediate steps of the CVD process, seen in Figure 4, have each been characterized by XRD—Figure 5 and UV/Vis—Figure 7. These samples were produced without the drying agent P_4O_{10} in the HI production step.

Figure 5 shows that in all steps of the CVD process a high amount of oriented MAPI forms, having a (100) reflex at 14.2°, a (200) reflex at 28.5°, and a (300) reflex at 43.4°, which indicates strong texturing of the samples. These values are in accord with literature.[19,20] Although from Equations 2 and 3 the formation of PbO and $Pb(OH)_2$ is expected, neither species can be found in the XRD patterns of the samples; however, XPS measurements (Figure S1) do indicate the formation of PbO and $Pb(OH)_2$. These species merely form on the surface of the samples, only being detected by the surface-sensitive XPS technique, or they could exist as amorphous phases, or having very small crystallites spread out throughout the material, that could make them undetectable by the bulk measuring method XRD.

Rietveld refinements of the XRD measurements displayed in Figure 6 (2.5 MA sample) indicate the presence of a mixture of a cubic and a tetragonal MAPI perovskite phase. Rietveld refinements of the samples 1.0. HI, 1.5 MA, and 2.0. HI (Figure S5-S7) also feature a mixture of the two phases. In contrast, the 0.5 MA sample from Figure S4 could be fitted with a cubic phase only. Results of the lattice parameters, phase fraction distributions, texture parameters, and volumes per ABX_3 unit are summarized in Table 1. The low values of the refined March-Dollase parameters, ranging from 0.16 to 0.21, indicate highly textured film growth with the (001) plane in parallel to the film surface. Two perovskite phases can be found within most of the films, indicated by the (400) reflection around 60° 2theta. These are high-volume phases, indicated to be predominantly tetragonal when found in high quantities, as well as a low-volume phase, predominantly cubic.[21] Their quantities show a strong dependence on the treatment step, where the low-volume phase becomes predominant after MA treatment.

The different phases with different volumes most likely indicate that the material can exist in different defect states with slightly different compositions.

Figure 7 shows UV/Vis spectra of samples of each step of the CVD process. The optical band gap E_g of the materials formed is red-shifted through the progressing cycles, from 1.61 eV (768 nm) for the PbI_2 layer that was treated only once with methylamine (0.5 MA), to 1.60 eV (773-774 nm) for the intermediate steps and finally 1.59 eV (778 nm) for the last step of the process (2.5 MA), indicating an increased amount of MAPI crystallinity. The band gaps are in accordance with literature values for MAPI.[22,23] The PL band of MAPI originates from a near-band-edge transition[24,25] and is with 1.63 eV (762 nm), for a 2.5 MA sample (Figure S3), higher than the measured optical band gap of 1.59 eV (778 nm).

FIGURE 4 Appearance of the different substrates with the stack of materials Glass/FTO/c-TiO_2/m-TiO_2/ MAPI, after each step of the chemical vapor deposition process
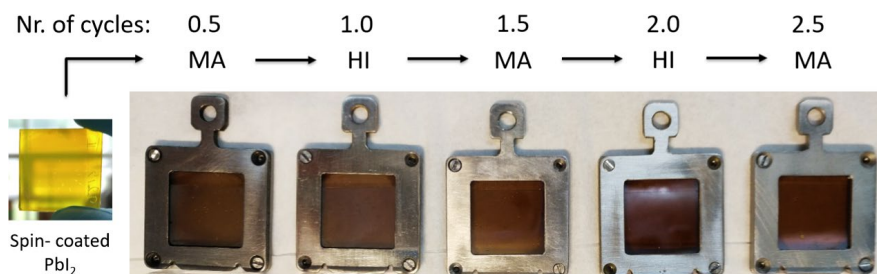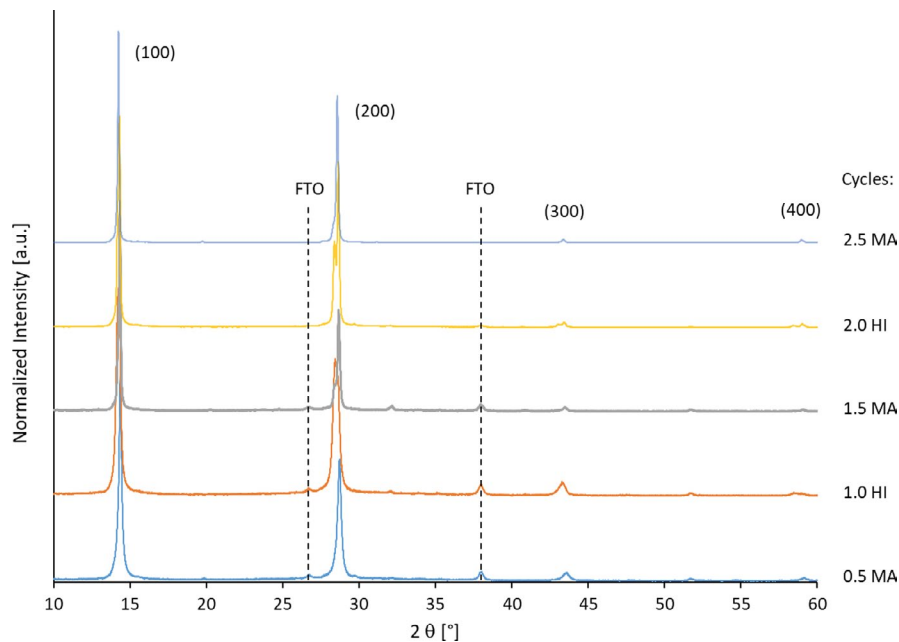
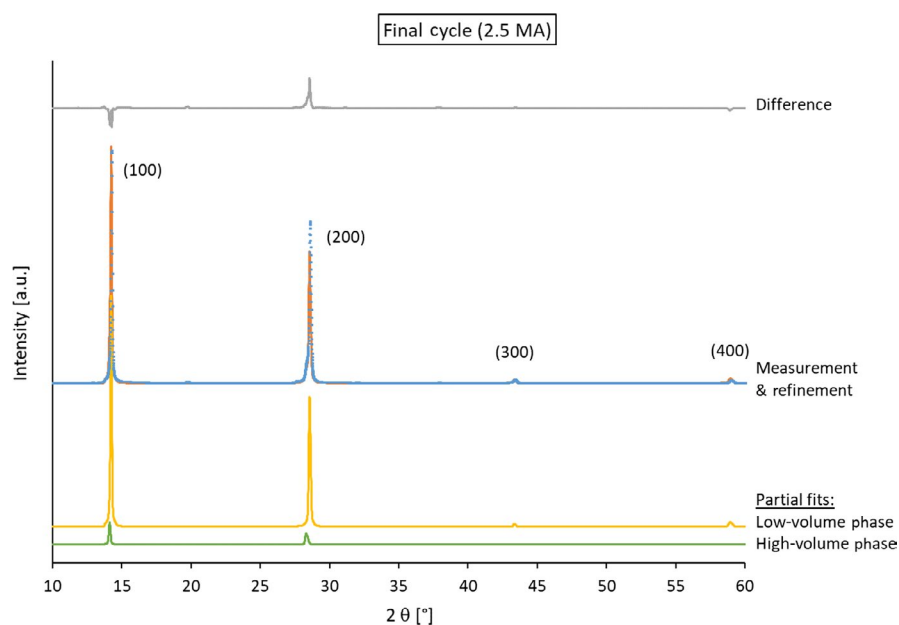**FIGURE 5** XRD patterns of the MAPI substrates from all intermediate steps of the CVD cycled process

FIGURE 6 XRD pattern and refinements of the substrate measured after the final cycle of the chemical vapor deposition process, 2.5 MA

TABLE 1 Refined parameters of the phases in the perovskite mixture produced in the cycles of the chemical vapor deposition process

		Low-volume phase			High-volume phase			
Sample	Texture parameter	a (Å)	Fraction (%)	Volume per ABX_3 unit (Å^3)	a (Å)	c (Å)	Fraction (%)	Volume per ABX_3 unit (Å^3)
0.5 MA	0.20	8.870 (7)	100	246.8	8.971 (7)	12.654 (8)	0	—
1.0 HI	0.21	8.901 (5)	31.5	249.3	8.967 (9)	12.614 (7)	68.5	254.6
1.5 MA	0.21	8.877 (7)	78.1	247.4	8.953 (0)	12.692 (0)	21.9	253.6
2.0 HI	0.19	8.883 (2)	65.2	247.5	8.950 (0)	12.610 (5)	34.8	254.3
2.5 MA	0.16	8.879 (0)	89.4	250.8	8.967 (9)	12.565 (2)	10.6	253.1
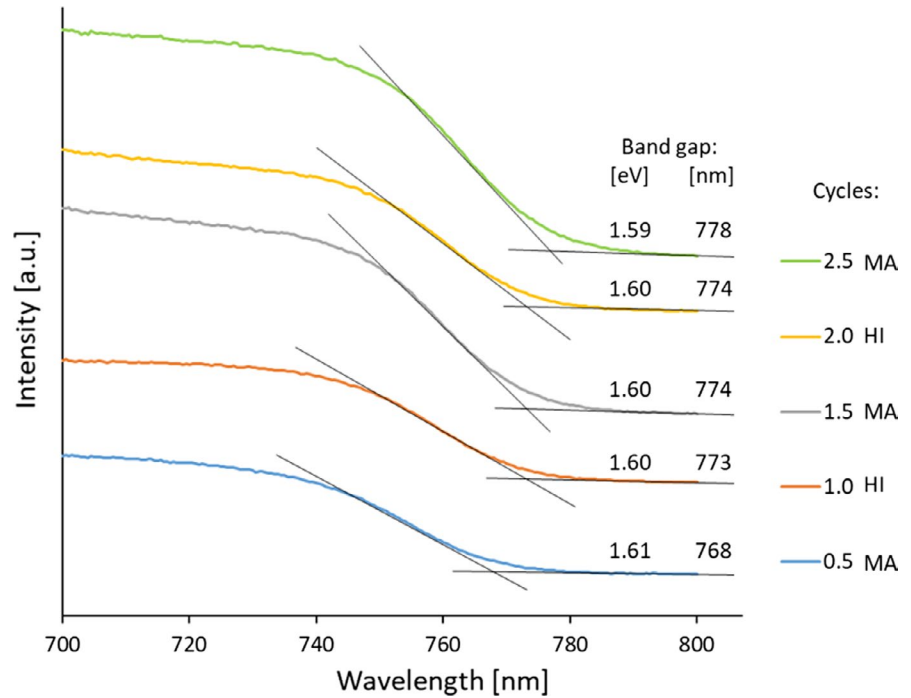
Solar cells of the CVD MAPI films use the stack sequence Glass/FTO/c-TiO$_2$/m-TiO$_2$/MAPI/spiro-MeOTAD/Gold, as illustrated in Figure 8, left. The substrates are 4 cm^2 in size, each holding four 32.5 mm^2 large cells. The cross-sectional SEM image of a completed cell, Figure 8, right, reveals a MAPI perovskite thick film of 400 nm, while the initial PbI$_2$ layer is 250 nm thick (Figure S2).

Figure 9 shows current-voltage curves of the champion cells under an AM1.5G illumination, measured with a scanning speed of 0.1 V/s, which were produced without and with the drying agent P$_4$O$_{10}$ in the HI step, respectively. The best solar cell produced with the drying agent reached a 12.9% efficiency under MPPT (maximum power point tracking), while the one without the drying agent reached an efficiency of 11.7%, each for a 32.5 mm^2 cell on a 4 cm^2 substrate.

The spread of the efficiencies of the solar cells made with the drying agent (HI production step) is 1.9% with an average of 11.1%, and the spread for the cells made without the drying agent is 1.4% with an average of 9.4%. The individual values for the efficiencies, the open circuit voltages (V_{OC}),

the short circuit currents (J_{SC}), and the fill factors for representative solar cells are given in Table 2. The low fill factors with an average value of around 60% may be related to PbO and Pb(OH)$_2$ species that have been found on the surface of the films by the XPS measurements presented in Figure S1.

6 | CONCLUSION

This work shows that an upscalable CVD process can be successfully employed to produce well-working thin film perovskite solar cells, with an efficiency of up to 12.9% for 2 × 2 cm^2 substrates and 32.5 mm^2 large cells, using a predeposited lead(II)iodide layer (PbI$_2$), methylamine gas (MA), and hydrogen iodide gas (HI). The method produces a mixture of highly oriented cubic and tetragonal perovskite material. One given limitation of the process is that the MAPI perovskite phase is nonpure, due to the nature of the mechanism, that involves water for the reaction and the by-products lead oxide (PbO) and lead hydroxide (Pb(OH)$_2$).

FIGURE 8 Left: schematic stack of materials used in the solar cells. Middle: photograph of a sample with solar cells and given dimensions. Right: cross-sectional SEM image of a completed solar cell. Sample tilted at 70°
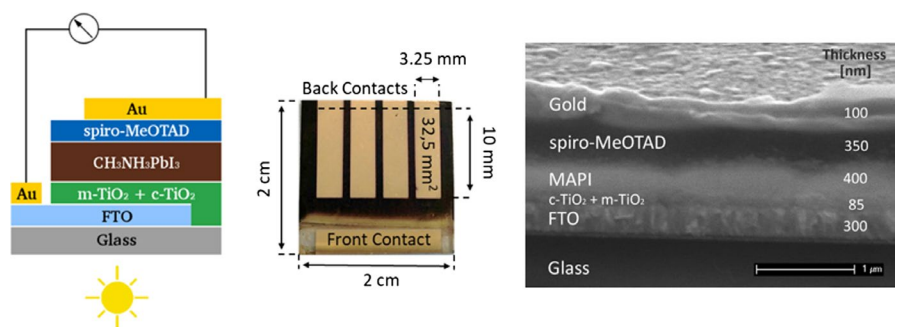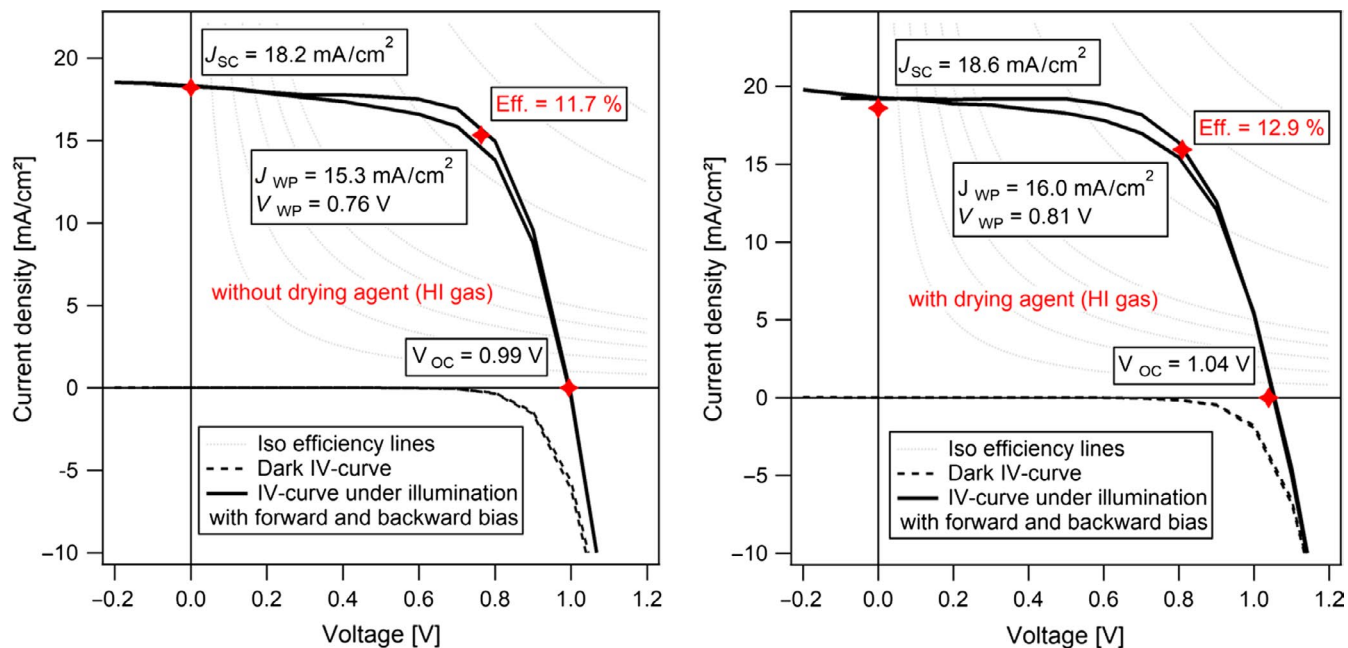
FIGURE 9 IV-curves of a solar cell from the CVD process with MPPT values; left: without using the drying agent for the HI step; right: using the drying agent for the HI step

TABLE 2 Solar simulator performance characteristics of different perovskite solar cells, built-up using the chemical vapor deposition process

	Cell	With drying agent (HI gas)				Without drying agent (HI gas)			
		Efficiency (%)	V_{OC} (V)	J_{SC} (A/m^2)	Fill factor (%)	Efficiency (%)	V_{OC} (V)	J_{SC} (A/m^2)	Fill factor (%)
Sample I	1	4.2	1.04	76	53	8.1	0.84	180	54
	2	11.8	1.06	176	63	10.1	1.01	170	59
	3	11.9	1.04	181	63	6.4	0.74	167	52
	4	10.3	1.03	175	57	10.0	1.02	144	68
Sample II	5	12.8	1.08	183	64	8.0	0.95	150	56
	6	11.8	1.04	173	65	**11.7**	0.99	182	65
	7	**12.9**	1.04	186	67	11.0	0.99	172	65
	8	12.8	1.04	188	65	9.6	0.98	161	61
	Average	11.1	1.05	167	62	9.4	0.94	166	60

Bold values—highest efficiencies achieved.

On the other hand, the process can be used in atmospheric conditions, using ambient, humid air. In addition, the process may be adapted to perovskite materials with more complex compositions.

CONFLICT OF INTEREST

The authors declare no competing financial interest.

ORCID

Claudiu Mortan https://orcid.org/0000-0002-5722-5943

REFERENCES

1. Kim HS, Lee CR, Im JH, et al. Lead iodide perovskite sensitized all-solid-state submicron thin film mesoscopic solar cell with efficiency exceeding 9%. *Sci Rep.* 2012;2:591.

2. Lee MM, Teuscher J, Miyasaka T, Murakami TN, Snaith HJ. Efficient hybrid solar cells based on meso-superstructured organometal halide perovskites. *Science*. 2012;338(6107):643-647.

3. Korea University. Chart of Best Research-Cell Efficiencies Provided by NREL. 2020. https://www.nrel.gov/pv/cell-efficiency.html

4. HZB. Chart of Best Research-Cell Efficiencies Provided by NREL. 2020. https://www.nrel.gov/pv/cell-efficiency.html

5. NREL. Chart of Best Research-Cell Efficiencies Provided by NREL. 2020. https://www.nrel.gov/pv/cell-efficiency.html

6. Shockley W, Queisser HJ. Detailed balance limit of efficiency of p-n junction solar cells. *J Appl Phys*. 1961;32(3):510-519.

7. Juarez-Perez EJ, Hawash Z, Raga SR, Ono LK, Qi YB. Thermal degradation of $CH_3NH_3PbI_3$ perovskite into NH_3 and CH_3I gases observed by coupled thermogravimetry-mass spectrometry analysis. *Energ Environ Sci*. 2016;9(11):3406-3410.

8. Baekbo MJ, Hansen O, Chorkendorff I, Vesborg PCK. Deposition of methylammonium iodide via evaporation – combined kinetic and mass spectrometric study. *Rsc Adv*. 2018;8(52):29899-29908.

9. Upadhyaya A, Negi CMS, Yadav A, Gupta SK, Verma AS. Synthesis and characterization of methylammonium lead iodide perovskite and its application in planar hetero-junction devices. *Semicond Sci Tech*. 2018;33(6):065012.

10. Weiss M, Horn J, Richter C, Schlettwein D. Preparation and characterization of methylammonium tin iodide layers as photovoltaic absorbers. *Phys Status Solidi A*. 2016;213(4):975-981.

11. Levchuk I, Hou Y, Gruber M, et al. Deciphering the role of impurities in methylammonium iodide and their impact on the performance of perovskite solar cells. *Proc SPIE*. 2016;3(22):9936.

12. Zhou ZM, Wang ZW, Zhou YY, et al. Methylamine-gas-induced defect-healing behavior of $CH_3NH_3PbI_3$ thin films for perovskite solar cells. *Angew Chem Int Ed Engl*. 2015;54(33):9705-9709.

13. Raga SR, Jiang Y, Ono LK, Qi YB. Application of methylamine gas in fabricating organic-inorganic hybrid perovskite solar cells. *Energy Technol*. 2017;5(10):1750-1761.

14. Dollase WA. Correction of intensities for preferred orientation in powder diffractometry – application of the March model. *J Appl Crystallogr*. 1986;19:267-272.

15. Furniss B, Hannaford A, Smith P, Tatchell A. Solvents and Reagents. *Vogel's textbook of practical organic-chemistry* (5th edn). 1989:439.

16. Raga SR, Ono LK, Qi YB. Rapid perovskite formation by CH_3NH_2 gas-induced intercalation and reaction of PbI_2. *J Mater Chem A*. 2016;4(7):2494-2500.

17. Shao ZP, Wang ZW, Li ZP, et al. A scalable methylamine gas healing strategy for high-efficiency inorganic perovskite solar cells. *Angew Chem Int Ed Engl*. 2019;58(17):5587-5591.

18. Zhao T, Williams ST, Chueh CC, et al. Design rules for the broad application of fast (< 1 s) methylamine vapor based, hybrid perovskite post deposition treatments. *Rsc Adv*. 2016;6(33):27475-27484.

19. Peng W, Miao XH, Adinolfi V, et al. Engineering of $CH_3NH_3PbI_3$ perovskite crystals by alloying large organic cations for enhanced thermal stability and transport properties. *Angew Chem Int Ed Engl*. 2016;55(36):10686-10690.

20. Baikie T, Fang YN, Kadro JM, et al. Synthesis and crystal chemistry of the hybrid perovskite $(CH_3NH_3)PbI_3$ for solid-state sensitised solar cell applications. *J Mater Chem A*. 2013;1(18):5628-5641.

21. Palazon F, Perez-del-Rey D, Danekamp B, et al. Room-temperature cubic phase crystallization and high stability of vacuum-deposited methylammonium lead triiodide thin films for high-efficiency solar cells. *Adv Mater*. 2019;31(39):e1902692.

22. Quarti C, Mosconi E, Ball JM, et al. Structural and optical properties of methylammonium lead iodide across the tetragonal to cubic phase transition: implications for perovskite solar cells. *Energ Environ Sci*. 2016;9(1):155-163.

23. Wang T, Daiber B, Frost JM, et al. Indirect to direct bandgap transition in methylammonium lead halide perovskite. *Energ Environ Sci*. 2017;10(2):509-515.

24. Kong WG, Ye ZY, Qi Z, et al. Characterization of an abnormal photoluminescence behavior upon crystal-phase transition of perovskite $CH_3NH_3PbI_3$. *Phys Chem Chem Phys*. 2015;17(25):16405-16411.

25. Yamada Y, Nakamura T, Endo M, Wakamiya A, Kanemitsu Y. Near-band-edge optical responses of solution-processed organic-inorganic hybrid perovskite $CH_3NH_3PbI_3$ on mesoporous TiO_2 electrodes. *Appl Phys Express*. 2014;7(3):032302.

SUPPORTING INFORMATION

Additional supporting information may be found online in the Supporting Information section.